Int. J. Electrochem. Sci., 17 **(2022)** Article Number: 221183, doi: 10.20964/2022.11.84

International Journal of
ELECTROCHEMICAL
SCIENCE
www.electrochemsci.org

Short Communication

First-principles Study and Experimental Preparation of $LiMn_2O_4$ Cathode Material Based on Spinel Structure

Xinghua Liang[1,], Dongxue Huang[1], Xun Yuan[2], Fangli Ji[3], Lingxiao Lan[1,*], Xingtao Jiang[1], Zhenjiang Wang[1], Zhijie Fang[1], Li Minghua[4]*

[1] Guangxi Key Laboratory of Automobile Components and Vehicle Technology, Guang University of Science & technology, Liuzhou 545006, China;
[2] Guangxi Zhongwei New Energy Technology Co., Ltd, Qinzhou 535000, China;
[3] Hunan Zhongwei New Energy Technology Co., Ltd, Changsha 410000, China;
[4] School of Electrical Technology, Guangdong Mechanical & Electrical Polytechnic, Guangzhou 510 515, China;
[*]E-mail: 309602373@qq.com

Received: 5 August 2022 / *Accepted:* 28 September 2022 / *Published:* 20 October 2022

Spinel-structured $LiMn_2O_4$ has three-dimensional lithium ion transport channels, and has become one o f the preferred materials for future high-energy and high-power lithium-ion batteries due to its high ope rating voltage, good stability, and low price. However, its capacity decays rapidly during charging, hind ering large-scale commercialization. In order to improve and enhance the cycling performance and cap acity of $LiMn_2O_4$, it is crucial to correctly understand the atomic properties of the microstructure. In thi s work, we use density functional theory to investigate the nature of lithium ions and the migration barr iers of lithium vacancies in spinel structures. The related compounds were prepared by the sol-gel meth od, and the battery was assembled to study the performance. The results show that the substitution of M n atoms in $LiMn_2O_4$ by various trivalent, tetravalent and pentavalent cations X (LXM) leads to structur al changes affecting Li mobility. The calculated activation energy of the migration vacancy is less than 0.026eV, and for the migration gap in $LiMn_2O_4$, the calculated migration energy is about 0.746eV. How ever, substitution by Ni and Al elements introduces interstitial Li ions for charge compensation, stabiliz ing the spinel structure and improving the ion transport of $LiMn_2O_4$. After experimental studies, it was also verified that the element doping improves the cycle.

Keywords: $LiMn_2O_4$;density functional theory; spinel structures; migration gap; ion transport

1. INTRODUCTION

Spinel-type cathode materials with three-dimensional lithium ion channels have received extensive attention from researchers at home and abroad. [1] The theoretical specific capacity is 148mAh/g, and the actual capacity is 110~130mAh/g. As a cathode material, it has the advantages of

rich manganese resources, high working voltage, good stability, low price and non-toxicity. [2-5] However, due to the Jahn-Teller effect, the dissolution of Mn^{3+} and the decomposition of the electrolyte, the capacity decays rapidly during the charge-discharge cycle, especially at high temperature. In addition, its storage performance and stability at high temperature are also relatively poor, hindering the further large-scale commercialization of spinel $LiMn_2O_4$. [6-8]

In order to improve and improve the cycling stability and capacity of $LiMn_2O_4$, researchers mainly conduct modification research by exploring the methods of material synthesis and preparation, and changing its structure. [9-10] Among them, element doping is one of the effective methods to improve the properties of $LiMn_2O_4$ materials. The electrochemical performance of the material can be effectively improved by incorporating appropriate transition metal X atoms in place of some Mn atoms. Through element doping, the performance of large capacity and high energy ratio is improved. [11] The doping of elements leads to changes in the surface of potential energy, which may change the barrier of lithium ion migration, and may also change the path of lithium ion migration. Therefore, It is very necessary to conduct in-depth research on the migration path of lithium ions in $LiMn_2O_4$ materials. Among the doping elements, we choose Al, which is common in the laboratory, based on the factors that are common in daily life and the price is relatively low. However, based on the choice of doping significance, we also choose Ni for doping, based on the reason that Ni can improve the voltage plateau seen in the literature. [12-13]

Spinel-type $LiMn_2O_4$ belongs to the cubic crystal system, which belongs to the Fd-3m space group, and the lattice constant a=8.221 Å. The $[Mn_2O_4]$ skeleton is a coplanar formed by the tetrahedral lattice 8a, 48f and the octahedral lattice 16c. [14-16] Three-dimensional channels, which are very favorable for the diffusion of Li^+. In the spinel structure, oxygen atoms occupy the 32e position, which is cubic close packing; manganese atoms occupy the 16d position, alternately located in the octahedral interstitial positions of the oxygen atoms close-packed; and lithium is located in the 1/8 oxygen tetrahedral interstitial (8a) position. [17-21] Therefore, Li ions are deintercalated in the Mn_2O_4 three-dimensional network structure along the 8a-16c-8a sequential path through the empty adjacent tetrahedral and octahedral interstitials. Shuttle location. They are alternately arranged along conductive channels and establish a three-dimensional migration network throughout the crystal structure. Some compositions with larger tetravalent cations also show a lower symmetrical triclinic phase due to displacement of Li ions. [22-25]

Ion migration in crystal structures is driven by thermally activated hopping of ions between interstitials or vacancies. [26-29] Also, macroscopic diffusion depends on the microstructure of the material. Extensive experimental investigations of Li^+ diffusion into the rhombohedral structure of $LiMn_2O_4$ and related materials have been carried out, and to our knowledge, $LiMn_2O_4$, $LiAl_{0.25}Mn_{1.75}O_4$ and $LiNi_{0.5}Mn_{1.5}O_4$ have been studied in atomic models using density functional theory (DET), moreover $LiAl_{0.25}Mn_{1.75}O_4$ and $LiNi_{0.5}Mn_{1.5}O_4$ have been shown to improve battery performance. [30-35] Lithium ion migration pathway. Partial substitution of Ni ions is carried out for a variety of elements, although structures with Ge etc. replacing Ni for Mn elements do stabilize metallic Li, they are significantly more expensive to produce and there are polymorphisms in structures with larger cations problem. Therefore, our DFT studies focus on the effect of cationic substitution on crystal structure and energy barriers compared to unsubstituted $LiMn_2O_4$. [36]

In-depth study of $LiMn_2O_4$ materials, it is necessary to correctly understand the basic physical properties of the atomic structure, and to deeply understand the conduction mechanism and the influence of defects on the material. In the following sections, the spinel structural model and computational DFT setup are described, the results are presented and discussed, and finally the conclusion is given. Then, on the basis of the experiment, we will understand the macroscopic results, use the first principles to explain theoretically and show the problems in the battery macroscopically in the experiment, so as to correctly understand the synthesis and modification of $LiMn_2O_4$ and play a guiding role.

2. THEORETICAL CALCULATIONS AND EXPERIMENTS

2.1. Structural model of the LMO

For the calculations, a conventional hexahedral unit cell with a spinel structure of 56 atoms was used. One Li atom is removed to create the vacancy required for diffusion. As a reference structure, the unsubstituted $LiMn_2O_4$ composition was chosen, and the LXMO composition of the remaining two cations (X = Ni, Al) substituted for Mn was calculated. Relaxation of unit cell volume and atomic positions was performed for each composition. By substituting only one of the sixteen Mn atoms with an X cation in the unit cell LXMO, the direct effect of lower concentrations of substituting elements on the diffusion path has been described. For these structures, only the atomic positions have been relaxed, and the relaxed unit constant of $LiMn_2O_4$ has also been used for all LXMO, since by replacing only one of the 16 Mn atoms in the unit cell, the volume changes are small. By doping LXMO with Al and Ni elements to change the potential barrier of lithium ion migration, the electrochemical performance of the material can be effectively improved.

2.2. Geometry optimization

In this paper, the calculation is performed in the VASP. This module studies the geometric structure of $LiMn_2O_4$ and LXMO unit cells based on density functional theory. In the calculation, the generalized gradient approximation (GGA-PBE) scheme is used to describe the exchange correlation energy between electrons and electrons.

2.3. calculation method

DFT calculations are performed using the VASP to express the wave function of valence electrons and ultrasoft pseudopotentials using a plane wave basis to describe the interaction of ion nuclei with valence electrons. The exchange correlation contribution is described by the generalized gradient approximation (GGA) of Perdew, Burke and Ernzerhof. The parameters in the calculation are set as follows: the optimization parameters including the interatomic interaction force, the convergence criterion is set to 0.02eV/Ang, the plane wave cutoff is set to 500eV, and the grid parameters are set to 5x5x5. The atomic maximum displacement convergence criterion is set to 1.0×10^{-5}μeV. The error

between the optimized value and the initial unit cell constant a set according to the experimental data is 1.8%. Relaxation of the unit cell volume is accomplished by minimizing the total energy, and the atomic positions are relaxed until the residual force acting on the atoms is less than 10^{-3} eV/Å.

2.4. Experiment preparation

Li_2CO_3 (analytical pure AR), $C4H_6MnO_4$•$4H_2O$ (analytical pure AR), anhydrous ethanol (analytical pure AR), Al_2O_3 (analytical pure AR), NiO (analytical pure AR) several materials. Li_2CO_3 and $C_4H_6MnO_4$•$4H_2O$ were weighed according to the stoichiometric ratio of 4:7, dissolved in absolute ethanol to obtain a pink mixed solution, stirred on a constant temperature magnetic stirrer for 5 hours, and then placed in a blast drying oven for drying. Pour the dried tan material into the agate grinding body and grind it for no less than 1 hour; put it in an atmosphere furnace and burn it at a temperature rate of 5°C/min to 350°C for 2 hours, and then heat it at a heating rate of 5°C/min. Raised to 900 ℃ and sintered for 18 hours to obtain, put into agate grinding body for grinding treatment to obtain spinel $LiMn_2O_4$. At the same time, it was prepared according to two chemical equations, $LiNi_{0.5}Mn_{1.5}O_4$ and $LiAl_{0.25}Mn_{1.75}O_4$, which were doped by Ni and Al in place of Mn in LXMO. [37-38] The resulting material is tested, and finally the battery assembly test is carried out.

3. RESULTS AND DISCUSSION

3.1. The structure of the unit cell system

In the spinel structure, oxygen atoms occupy the 32e position, which is cubic close packing; manganese atoms occupy the 16d position, alternately located in the octahedral interstitial positions of the oxygen atoms close-packed; and lithium is located in the 1/8 oxygen tetrahedral interstitial (8a) position Figure 1a. [39] In this triclinic structure, lithium ions intercalate and move out of Li^+ according to the 8a-16c-8a channel. Considering the changes in the crystal structure of doping elements and the migration of lithium ions, the effect of doping on the migration of lithium ions Influence, we calculate the migration in the A to B direction, and the migration path of Li ions in spinel is given in Fig. 1b, assuming the yellow unit cell as the replacement element. Observe the effect of doping elements on lithium ions during the migration from A to B. At the same time, for the convenience of identification, we put $LiMn_2O_4$, $LiNi_{0.5}Mn_{1.5}O_4$ and $LiAl_{0.25}Mn_{1.75}O_4$, are labeled as LMO, LNMO and LAMO.

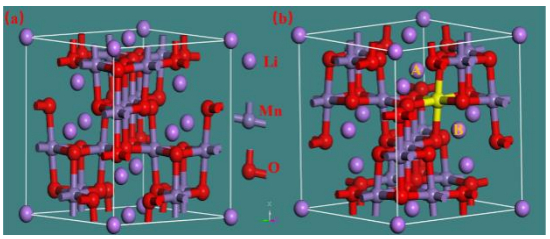

Figure 1. a）Optimized LMO cell structure, b）the migration path of the unit cell structure

3.2. Energy band and density of states of the unit cell system

In the first-principles calculation, we optimized the unit cell structure of several materials, and then obtained the energy band and density of states diagrams, where the abscissa of the energy band structure diagram is the node (Fig. 2a.b.c), and the It is called the high symmetry point of the reduced Brillouin zone, the ordinate represents the energy, and the Fermi energy is set at the zero point of the abscissa. The peak density of states increases slightly, which increases its bonding degree and the structural system becomes more stable. [40] At the same time, the energy system is reduced to a certain extent, the upper valence band becomes wider, so that the fermi energy level enters the upper valence band, and the valence band becomes an unsatisfactory band after doping Al element and Ni element, which reduces the energy band gap, which corresponds to the impedance in the following experiments. The results are consistent, speeding up the mobility of electrons and enhancing the mobility of Li^+.

The energy band is mainly concentrated at -43.85~0.33eV, the valence band is at -45~-1eV, and the conduction band is at 1~-20eV. After doping Al element and Ni element, the gap between the highest occupied orbital and the lowest empty orbital is smaller than that of LMO, such a small energy band gap is beneficial to improve the electronic conductivity of the material, and the energy required for electrons to transition from the valence band to the conduction band is relatively small. [41] The energy band density from -7.36eV to -1eV is very obvious. At the same time, it is close to the Fermi level, and the corresponding density of states peak is also very significant, indicating that this region of the valence band is the main bonding region, and the conduction band region is The main antibonding region. The energy transition after doping Al element and Ni element are reduced and the conductivity is improved.

The figure is Fig. 2d, e and f are the density of states of LMO, LAMO and LNMO, the abscissa is the energy, and the ordinate is the density of states. With the replacement of elements, the peaks near the LAMO Fermi level are mainly contributed by Al-p, O-s and Mn-d electron orbitals, and the electron orbits of Mn and O elements overlap significantly, indicating that doping Al element and Ni element improves the interaction between elements and the stability of the unit cell structure. The total density of states peak near -20eV is mainly provided by the O-2s electron orbital, and this peak is very sharp, indicating that the bonding effect is small, the anti-bonding effect is strong, and the localization is obvious. Since the radius of Al is smaller than that of Mn, the original Mn The bond length of O is shortened, which is beneficial to improve the structural stability of the Mn-O framework. The intensity of the total density of states peak near -44eV is mainly provided by the Li-1s orbital, and the area integral of this peak is 2, which indicates that the peak is completely provided by two electrons in the Li-1s electron orbital. The peak is sharp, and the total state The peak intensity of the density near the Fermi energy has no contribution from Li, indicating that the interaction between Li and Mn-O is very weak, and Li can shuttle and de-intercalate freely in the Mn-O structure, which facilitates the transfer of lithium ions, indicating that this material is suitable as a cathode material for lithium-ion batteries. [42] Compared with article, the doping Al element and Ni element improves the stability of the unit cell structure compared to other element-doped unit cell structures. [43-44]

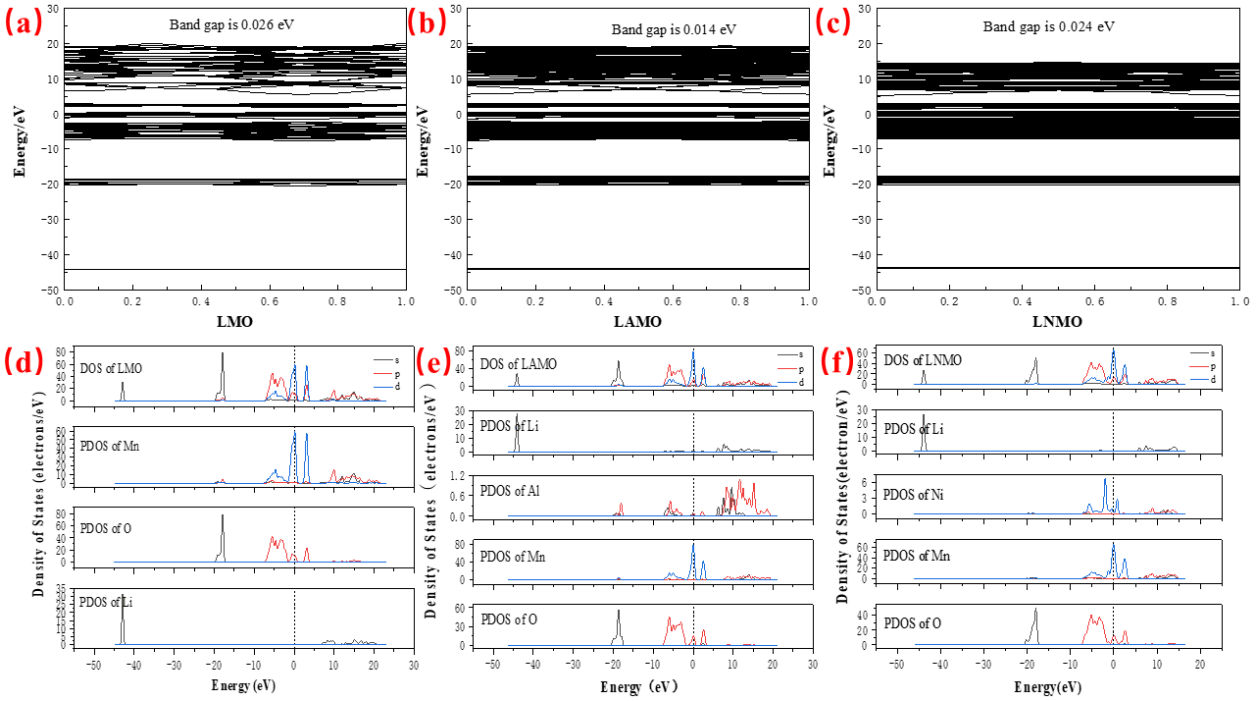

Figure 2. Band structure and total density and states diagrams of LMO、LAMO and LNMO.

3.3 Bulk phase migration of the structure of the unit cell

The opposite migration of the two sites was calculated separately, and the migration energy barrier was the same (Fig. 3), which was 0.746 eV, so it was assumed that the migration from the A site to the B site was. We first calculated the effect of the undoped position on the migration of lithium ions. When the A and B position in the LMO unit cell structure, we first established two unit cell structures, named product and reactant, and the migration energy barrier required to calculate the interstitial migration was 0.746 eV, and then, we study again the energies required for the migration of the two sites A and B after Al and Ni atoms replace Mn in LXMO for doping, respectively. The calculated results are 0.57 eV and 0.32 eV, respectively. The replaced atoms make the migration of nearby lithium ions more It is easy to draw the reason, which is due to the fact that the lithium ion is bound by the Mn atom, and the distance is short, and it is greatly affected by the Mn atom. The effect is small, making it easy to shuttle in the unit cell structure. This is compared with the article, which requires less energy for the migration energy barrier comparison of doping elements. [45-46]

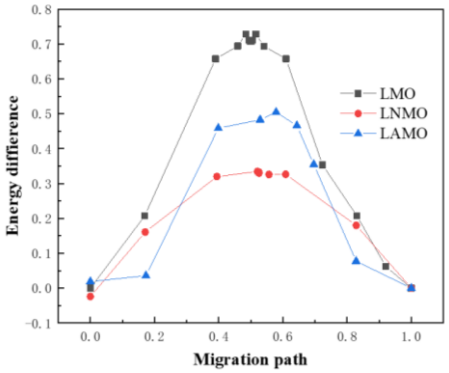

Figure 3. Migration barrier map

3.4 Experimental conclusion

From Figure 4a, b and c, it can be seen that the particle diameter distribution of the unit cell structure particles of LMO, LAMO and LNMO prepared by the sol-gel method is small and uniform, indicating that the sol-gel method The prepared lithium manganate is ideal, and has good conductivity uniformity as a positive electrode material. Figure 4d shows the comparison of the XRD diffraction patterns of the three materials prepared LMO, LAMO and LNMO. It can be seen that the three main peaks of the two materials LAMO and LNMO are basically consistent with the LMO pattern, indicating that the unit cell structures we prepared are all spinel structures. The doping Al element and Ni element did not change the morphology. However, in addition to the obvious main peak, there are different small peaks in the LMO, indicating that the doping of elements has changed the electronic structure in the unit cell, resulting in some changes in performance. [47]

To further demonstrate the effect of doping elements on the unit cell structure, we installed batteries for performance testing. As shown in Figure 4e, the assembled impedance map, with the doping of Al element, we can clearly see that the interfacial resistance of LAMO cells is smaller, and the interfacial resistance of LMO cells is larger Which is consistent with literature [48]. And at the same time, this is consistent with the previously calculated migration energy barrier, smaller interface impedance favors Li^+ migration within the unit cell structure with element doping. As we compare for 50 cycles, the stability of the unit cell structure after Al element doping is enhanced, which is manifested in that the cycle stability is stronger than that of LMO. And with the doping of Ni element, our unit cell structure also changes, the cycling stability of LNMO is also improved, although the specific capacity is not as high as that of LMO, we attribute this reason to the lack of a suitable high-voltage electrolyte. [49-50]

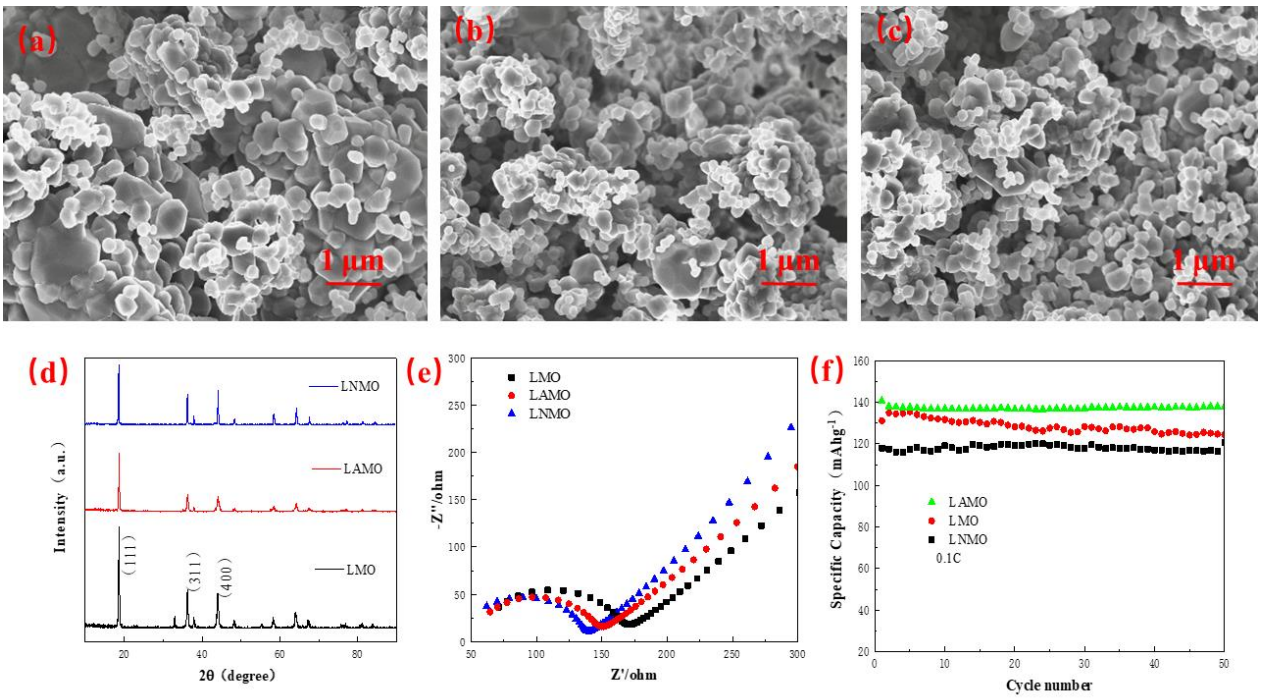

Figure 4. a.b.c SEM of LMO、LAMO and LNMO. d）XRD patterns of LMO、LAMO and LNMO. e）impedance diagram at LMO、LAMO and LNMO.f）50 cycles of LMO、LAMO and LNMO. battery

4. CONCLUSIONS

After element doping, the X-O bond length in the octahedron centered on the doping element increases compared with the Mn-O bond length. In the lattice, only the migration of lithium ions at the doping position is calculated, and the migration energy barrier is calculated. It can be seen from the calculation that after the element replaces the Mn^{2+} ion, the energy energy of the transition state after doping is reduced, and the migration barrier is smaller. The energy transition after doping is reduced and the conductivity is improved. We prepared three materials of LMO, LAMO and LNMO through experiments and assembled the battery. From a macroscopic point of view, it was shown that the doping of elements changed the properties of the LMO unit cell structure and improved the cyclic stability performance.

ACKNOWLEDGEMENTS
This research was supported by the Guangxi Innovation Driven Development Project (No.AA18242036-2), Guangxi Natural Science Foundation (No. 2020GXNSFAA297082), National Natural Science Foundation of China(No.52161033,52165055), the Fund Project of the GDAS Special Project of Science and Technology Development Guangdong Academy of Sciences Program (No.2020GDASYL-20200104030); The Innovation Project of Guangxi University of Science and Technology Graduate Education (YCSW2021324,GKYC202112) and the Fund Project of the Key Lab of Guangdong for Modern Surface Engineering Technology(No. 2018KFKT01); Featured Innovation Projects (Natural Science) of General Universities in Guangdong Province (Grant No. 2018GKTSCX082).

References

1. K.J. Lee, E.J. Yi, G. Kim and H. Hwang, *J. Nanosci. Nanotechnol.,* 20 (2020) 4494.
2. Y.M. Jin, C.J. Liu, X. Zong, D. Li, M.Y. Fu, S. Tan, Y.P. Xiong and J.H. Wei, *J. Power Sources,* 460 (2020) 228125.
3. M.D. Singh, A. Dalvi, D.M. Phase and Y. Kumar, *J. Mater. Sci.,* 55 (2019) 3951.
4. J. Guerra, C. Wayne, T. Musambe and N. Ahmed, *J. Pediatr. Surg.,* 51 (2016) 770.
5. K. Waetzig, A. Rost , U. Langklotz, B. Matthey and J. Schilm, *J. Eur. Ceram. Soc.,* 36 (2016) 1995.
6. J.M. Lim, R.G. Oh, D. Kim, W. Cho, K. Cho, M.Cho and M.S Park, *Chemsuschem,* 9 (2016) 2967.
7. G. Singh, S.L. Gupta, R. Prasad, S. Auluck, R. Gupta and A. Sil, *J Phys Chem Solids,* 70 (2009) 1200.
8. Z.X. Nie, C.Y. Ouyang, J.Z. Chen, Z.Y. Zhong, Y.L. Du, D.S. Liu and M.S. Lei, *Solid State Commun,* 150 (2010) 40.
9. X.F. Ouyang, M.L. Lei, S.Q. Shi, C.L. Luo, D.H. Liu, D.Y. Jiang, Z.Q. Ye and M.S. Lei, *J. Alloy Compd.,* 476 (2009) 462.
10. T. Hashimoto, S. Ishibashi and K. Terakura, *Phys. Rev. B,* 82 (2010) 045124.
11. H.K. Tian, R. Jalem, B. Gao, Y. Yamamoto, S. Muto, M. Sakakura, Y. Iriyama and Y. Tateyam, *ACS Appl. Mater. Inter,* 12 (2020) 54752.
12. F. Ning, B. Xu, J. Shi, M. Wu, Y. Hu and C. Ouyang, *J. Phys. Chem. C,* 120 (2016) 18428.
13. Liu,J.G. Wu,W. Zhao, J.L. Chu and T. Qi, *Chinese J. Chem.,* 031 (2013) 1257.
14. Z.L. Yang, H.Y. Yuan, C.J. Zhou, Y.M. Wu, W.P. Tang, S.B. Sang and H.T. Liu, *Chem. Eng. J.,* 392 (2020) 123650.
15. S. Shi, D.S. Wang, S. Meng, L. Chen and X. Huang, *Phys. Rev. B,* 67 (2003) 11513.
16. C.C. Yang, J.R. Jiang, C. Karuppiah, J.H. Jang, Z.H. Wu, R. Jose and S.J.J. Lue, *J. Alloy Compd.,* 765 (2018) 1256.
17. H. Luo, P. Nie, L. Shen, H. Li, H. Deng, Y. Zhu and X. Zhang, *ChemElectroChem,* 2 (2015) 127.
18. Y.M. Li, Q. Zhang, B.Y. Liu, B. McLellan, Y. Gao and Y.Y. Tang, *Energy,* 152 (2018) 223.
19. N.A. Kasti, *Sol Energy,* 144 (2017) 619.
20. Y.M. He, C.Y. Lu, S. Liu, W.J. Zheng and J.Y. Luo, *Adv. Energy Mater.,* 9 (2019) 1901810.
21. R. Murugan, V. Thangadurai and W. Weppner, *Angew. Chem. Int. Ed.,* 46 (2007) 7778.
22. V. Thangadurai, H. Kaack and W.J.F. Weppner, *J. Am. Ceram. Soc.,* 86 (2003) 437.
23. R. Jalem, M. J. D. Rushton, Jr. W. Manalastas, M. Nakayama, T. Kasuga, J. A. Kilner and R. W. Grimes, *Chem. Mater.,* 27 (2015) 2821.
24. L. Dhivya, N. Janani, B. Palanivel and R. Murugan, *Aip Adv.,* 3 (2013) 082115.
25. L. Wang, D. Chen, J. Wang, G. Liu, W. Wu and G. Liang, *Powder Technol.,* 292 (2016) 203.
26. J. Sun, Q. Mu, T. Wang, J. Qi and C.Hu, *J. Colloid Interface Sci.,* 590 (2021) 539.
27. R. Mücke, M. Finsterbusch, P. Kaghazchi, D. Fattakhova-Rohlfing and O. Guillon, *J. Power Sources,* 489 (2021) 229430.
28. Y. Liang, Y. Liu, D. Chen, L. Dong, Z. Guang, J. Liu, B. Yuan, M. Yang, Y. Dong, Q. Li, C. Yang, D. Tang and W. He, *Mater. Today Energy,* 20 (2021) 100694.
29. J.H Li and R.G. Wang, *Ceram. Int.,* 47 (2021) 13280.
30. R. Gonçalves, P. Sharma, P. Ram, S. Ferdov, M.M. Silva, C.M. Costa, R.Singhal, R.K. Sharma, S. Lanceros-Méndez, *J. Alloys Compd.,* 853 (2021) 157208.
31. K. Amine, H. Tukamoto, H. Yasuda, Y. Fujita, *J. Power Sources,* 68 (1997) 604.
32. T.Ohzuku, S. Takeda, M. Iwanaga, *J. Power Sources,* 81-82 (1999) 90.
33. M.A. Kebede, M.J. Phasha, N. Kunjuzwa, M.K. Mathe and K.I. Ozoemena, *Appl. Phys. A,* 121 (2015) 51.
34. M.A. Kebede, M.J. Phasha, N. Kunjuzwa, L.J.L. Roux, D. Mkhonto, K.I. Ozoemena, M.K. Mathe, *Sustain Energy Techn,* 5 (2014) 44.
35. R. Thirunakaran, A. Sivashanmugam, S. Gopukumar, C.W. Dunnill, D.H. Gregory,

J Phys Chem Solids, 69 (2008) 2082.
36. Y. Hakgyoon, J.S. Han, H.G. Chan, C.J. Sang and J.K. Sang, *Electrochim. Acta*, 365 (2021) 137349.
37. W.J. Qu, M.X. Yan, R. Luo, J. Qian, Y. Wen, N. Chen, L. Li, F. Wu and R.J. Chen, *J. Power Sources*, 484 (2021) 229195.
38. M. Shahi, F. Hekmat and S. Shahrokhian, *J. Colloid Interface Sci.*, 585 (2021) 750.
39. X. Li, J. Wang, S. Zhang, L. Sun, W. Zhang, F. Dang, J.S. Hans and Y. Du, *ACS omega*, 6 (2021) 21255.
40. H. Li, Y. Wang, G.L. Liu, L. Wei and D. Wang, *J Mol Model*, 28 (2022) 93.
41. M. Momeni, H.Y. Mashhour, Mohammad and M.M. Kalantarian, *J. Alloys Compd*, 02 (2019) 155.
42. Y.Y. Ma, L. lv, Y.W. Dai, Q.H. Zhou, J.M. Chen, H.L. Li and W. Hu, *J. Electron. Mater.*, 51 (2022) 77
43. Y. Sun, K. Suzuki, S. Hori, M. Hirayama and R. Kanno, *Chem. Mater.*, 29 (2017) 5858.
44. J. Ma, B.B. Chen, L.L. Wang and G.L. Cui, *J. Power Sources*, 392 (2018) 4.
45. Y. Seino, T. Ota, K. Takada, A. Hayashi and M. Tatsumisago, *Energy Environ. Sci.*, 7 (2014) 627.
46. N. Kamaya, K. Homma, Y. Yamakawa, M. Hirayama, R. Kanno, M. Yonemura and A. Mitsui, *Nat. Mater.*, 10 (2011) 682.
47. J.T. Liu, G. Li, Y. Yu, H.L. Bai, M.M. Shao, J.M. Guo, C.W. Su, Xi.F. Liu and W. Bai, *J. Alloys Compd.*, 728 (2017) 1315.
48. W. Xu, Y. Zheng, Y. Cheng, R. Qi, H. Peng, H. Lin and R. Huang, *ACS Appl. Mater. Interfaces*, 13 (2021) 45446.
49. Y.N. Zhang, Y.J. Zhang, M.Y. Zhang, M.L. Xu, X. Li, X.H. Yu and P.Dong, *JOM*, 71 (2019) 608
50. S.Yang, D. Schmidt, A. Khetan, F.Schrader, S.Jakobi, M. Homberger, M. Noyong, A. Paulus, H. Kungl, R.A. Eichel, H. Pitsch and U. Simon, *Materials*, 11 (2018) 806.